Observations of Three-Dimensional Radiative Effects that Influence MODIS Cloud Optical Thickness Retrievals

TAMÁS VÁRNAI AND ALEXANDER MARSHAK

Joint Center for Earth Systems Technology, NASA Goddard Space Flight Center, Greenbelt, and University of Maryland, Baltimore County, Baltimore, Maryland

(Manuscript received 14 May 2001, in final form 7 September 2001)

ABSTRACT

When cloud properties are retrieved from satellite observations, current calculations apply one-dimensional (1D) theory to the three-dimensional (3D) world: they consider only vertical processes and ignore horizontal interactions. This paper proposes a novel approach that estimates 3D effects in cloud optical thickness retrievals. The proposed method combines visible and thermal infrared images to see whether 3D radiative effects make clouds appear asymmetric—that is, whether cloud surfaces tilted toward the sun are systematically brighter than surfaces tilted away from it. The observed asymmetries are then used to estimate 3D effects for 1-km-size pixels as well as 50-km-size areas. Initial results obtained for Moderate-Resolution Imaging Spectroradiometer (MODIS) images reveal that 3D effects cause abundant uncertainties in the 1-km-resolution 1D retrievals. Averaging over 50 km by 50 km areas greatly reduces the errors but does not remove them completely. Conservative estimates show that the mean optical thickness values are biased by more than 10% in 10% of the areas, and the errors in the areas' standard deviation values are more than 10% in about 20% of areas.

1. Introduction

Satellites offer excellent opportunities to measure how much solar radiation clouds reflect and how much infrared radiation they emit. This information is often used to retrieve various cloud properties that influence the measured radiation, for example, the clouds' optical thickness or water content. For practical reasons, current retrieval techniques are based on one-dimensional (1D) radiative transfer theory—so they do not consider the radiative effects of horizontal cloud variability. Theoretical studies (e.g., Davies 1984; Kobayashi 1993; Barker and Liu 1995), however, have long suggested that three-dimensional (3D) radiative effects cause a wide variety of problems in the retrievals that do not consider them. Such studies (e.g., Marshak et al. 1995a; Zuidema and Evans 1998; Várnai 2000) have shown that—depending on the solar elevation, cloud structure, and satellite resolution—1D retrievals can estimate clouds to be too thin or thick, too smooth or rough, artificially anisotropic, and asymmetric. The main difficulty in interpreting such theoretical results is in figuring out which of the simulated cloud structures are typical in the real atmosphere, and so which of the calculated 3D effects are important in practice. Observational studies helped clarify this issue to some degree. They showed that 3D effects can make clouds appear too smooth or rough in high-resolution satellite images (e.g., Marshak et al. 1995a; Davis et al. 1997; Oreopoulos et al. 2000) and too thick in images of any resolution when the sun is very oblique (Loeb and Davies 1996; Loeb and Coakley 1998). Still, it is not yet clear how important 3D effects are in general, that is, how often they are strong enough to cause significant problems. The main difficulty lies in the lack of methods that could detect the presence of 3D effects in individual satellite images (except for detecting the small-scale radiative smoothing mentioned above).

Recently, Várnai and Marshak (2001) used theoretical simulations to examine the statistical behavior of 3D effects. For stratocumulus clouds they set statistical error bounds that estimate the uncertainties in cloud optical depth retrievals caused by 3D radiative effects. The present paper goes further: it presents a new technique that estimates the influence of 3D effects in satellite images by combining visible and infrared measurements. The proposed technique is then used to estimate the frequency of 3D effects in a set of images taken by the Moderate-Resolution Imaging Spectroradiometer (MODIS) instrument. This instrument (launched on the *Terra* satellite in December 1999) takes measurements at 36 wavelengths between 0.4 and 14 μm, with a spatial resolution of either 250 m, 500 m, or 1 km, depending on the wavelength. Because estimates of 3D effects reflect the accuracy of 1D retrievals (which do not con-

Corresponding author address: Tamás Várnai, Code 913, NASA GSFC, Greenbelt, MD 20771.
E-mail: varnai@climate.gsfc.nasa.gov

sider these effects), the results can be used to set error bounds on the operational MODIS cloud optical thickness product (Nakajima and King 1990; King et al. 1997).

The outline of this paper is as follows. Section 2 describes the MODIS data we used. Section 3 then describes a simple and robust technique to detect 3D effects over large areas, and section 4 gives some statistics on the frequency of these effects in MODIS images. Section 5 outlines a more refined technique that allows us to remove systematic biases by estimating 3D effects even for individual pixels, and section 6 discusses some results obtained by this technique. Section 7 offers a brief summary and some concluding remarks.

TABLE 1. Dates and measurement times that identify the data granules used in this study.

Set 1 ($\Theta_0 \approx 30°$)	Set 2 ($\Theta_0 \approx 65°$)
2325 UTC 1 Nov 2000	1305 UTC 1 Nov 2000
2340 UTC 4 Nov 2000	1335 UTC 4 Nov 2000
1420 UTC 7 Nov 2000	0055 UTC 7 Nov 2000
2045 UTC 11 Nov 2000	2200 UTC 11 Nov 2000
2255 UTC 14 Nov 2000	2230 UTC 14 Nov 2000
1830 UTC 17 Nov 2000	1445 UTC 17 Nov 2000
0300 UTC 23 Nov 2000	2015 UTC 20 Nov 2000
1930 UTC 23 Nov 2000	0235 UTC 23 Nov 2000
1450 UTC 26 Nov 2000	1300 UTC 26 Nov 2000
0225 UTC 29 Nov 2000	0200 UTC 29 Nov 2000

2. MODIS data used

This study uses radiance values measured by the MODIS instrument on board the *Terra* satellite at 2 of the 36 MODIS wavelengths, 0.86 and 11 μm. The 0.86-μm radiances are converted to reflectances (R) using the equation

$$R = \frac{\pi I}{\cos\Theta_0 F_0}, \tag{1}$$

where I is the radiance, Θ_0 is the solar zenith angle, and F_0 is the solar constant. The 11-μm radiances were transformed into equivalent brightness temperature (T) values using the Planck formula (e.g., Thomas and Stamnes 1999, p. 94).

Although other instruments [such as the Advanced Very High-Resolution Radiometer (AVHRR)] also give measurements at similar wavelengths, MODIS offers unique opportunities to detect 3D effects because of its excellent radiometric performance. Especially important is the sensitivity at 11 μm, where temperature differences as small as 0.01 K are reported in the images, and the noise equivalent temperature difference is about 0.05 K (NASA 2000). This high sensitivity allows us to detect very small temperature changes that, as described in the next section, are crucial for the proposed technique.

In addition to actual measurements, this study also uses the MODIS operational cloud products, particularly the 1-km-resolution cloud optical thickness values and the geolocation parameters.

MODIS data are distributed in 2030-km-long segments called granules. We used two sets of 10 granules that we selected randomly from November 2000. The dates and measurement times of the granules are listed in Table 1. The only criteria in the selection of granules were that the central portion of the granule should cover mostly oceanic areas and that the solar zenith angle at the center of the granule should be 25°–35° and 60°–70° in the two sets, respectively. The granules with low solar zenith angles are around the 15°N and 40°S latitudes, whereas the granules with high solar zenith angles are around 45°N latitude. For the sake of simplicity, we will refer to the two groups of granules with different solar zenith angles as $\Theta_0 = 30°$ and 65°, even though the solar zenith angles in the used portions of the granules can vary by almost $\pm 10°$.

Although MODIS takes measurements in an approximately 2000-km-wide swath, this study uses only the central 450-km-wide portions of the swaths, where the viewing zenith angle is less than about 20°. This restriction eliminates potential difficulties that could arise for oblique views near the swath edges, such as areas being viewed twice or pixel sizes increasing.

3. A technique to detect 3D radiative effects over large areas

This section describes a simple method to determine whether clouds in a $(50\ \text{km})^2$ area are influenced by 3D effects. We chose the $(50\ \text{km})^2$ size somewhat arbitrarily, with the goal that the areas contain many pixels for statistical calculations but that they not contain clouds from different cloud fields too often. The method's basic idea is to estimate, for each $(1\ \text{km})^2$ pixel in the area, whether 3D effects are likely to have increased or decreased the pixel's brightness at 0.86 μm (relative to 1D theory). Then we calculate the mean brightnesses of the pixels brightened and darkened by 3D effects. If the two mean values are nearly equal, we say that 3D effects do not make a difference. If, however, the average brightness is much larger for brightened pixels than for darkened pixels, we conclude that 3D effects are significant.

The proposed technique assumes that the question of whether 3D effects enhance or reduce the brightness of a pixel depends mainly on whether the pixel is on a slope tilted toward or away from the sun. For simplicity, we call these slopes *illuminated* and *shadowy*, respectively, even though no actual shadows are required for a pixel to be designated as shadowy.

Specifically, step 1 of the technique is to use the available geolocation data to determine from which direction the sun illuminates the area of a pixel, and thus, which neighboring pixels are closest to the solar azimuth in front of it and behind it (Fig. 1). The technique ex-

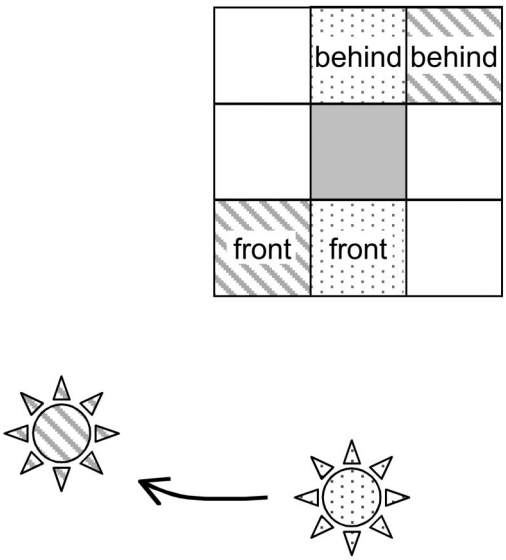

FIG. 1. Illustration of which neighboring pixels are considered for estimating 3D effects at the gray central pixel.

amines all cloudy pixels, that is, all pixels for which the operational MODIS data processing retrieved a nonzero cloud optical depth.

Step 2 then determines whether the pixel is on a slope tilted toward or away from the sun, that is, whether it is on an illuminated or shadowy slope. The determination uses the local gradient of brightness temperatures (g) calculated from the pixels in front and behind:

$$g = \frac{T_{\text{front}} - T_{\text{behind}}}{d}, \tag{2}$$

where d is the distance separating the pixels in front and behind (either 2 km or $2\sqrt{2}$ km). Because temperature tends to decrease with altitude, one can say that a pixel is on an illuminated slope if $g > 0$ and is on a shadowy slope if $g < 0$ (Fig. 2). This procedure designates pixels as illuminated or shadowy even if they lie at a local minimum or maximum. Test results indicated that excluding them would change the results only to a very small degree.

Once all cloudy pixels in a (50 km)^2 area are designated as either illuminated or shadowy, step 3 calculates the mean 0.86-μm brightness of the illuminated ($\overline{R}_i$) and shadowy ($\overline{R}_s$) pixels. [The overbar indicates averaging over all relevant pixels inside a (50 km)^2 area.] If the two mean values are close to each other, this indicates that 3D effects do not make much of a difference in the (50 km)^2 area. If, however, $\overline{R}_i$ is much larger than $\overline{R}_s$, 3D effects are expected to be strong.

In essence, this technique detects the asymmetry effect that was described by Várnai (2000) for some theoretical simulations of high-resolution satellite images. The detected effect is also the cause for the roughening discussed by Zuidema and Evans (1998) and Oreopoulos et al. (2000).

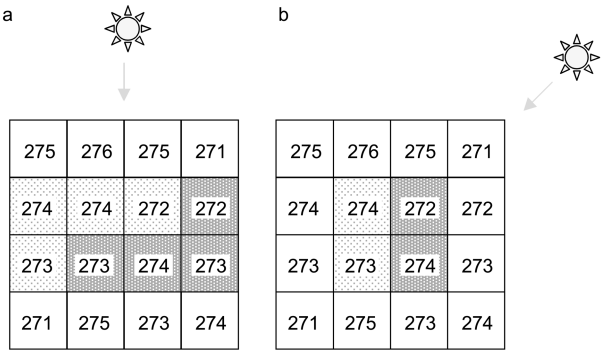

FIG. 2. An example of how pixels are designated as illuminated (light shading) or shadowy (dark shading). Each pixel's brightness temperature is displayed in Kelvins. Note that a pixel's designation can change from (a) to (b), as the sun moves to a different azimuth. The available information is not sufficient to make a designation for the pixels that are left without shading.

This simple technique has three main limitations: (i) it assumes that clouds are statistically symmetric, (ii) it detects only one component of the overall 3D effects, and (iii) it assumes that the cloud slope always determines whether a pixel is brightened or darkened by 3D effects. Let us conclude this section by discussing these limitations in detail.

The first limitation originates from the assumption that the solar azimuth does not influence cloud development, and so the illuminated and shadowy slopes have statistically similar cloud properties. At this point there is no evidence to contradict this assumption by suggesting any systematic differences between the properties of illuminated and shadowy slopes. Naturally, random processes (such as wind shear or the overlap of two cloud layers) can make clouds asymmetric in any particular (50 km)^2 area, but these effects should even out when a large number of areas are considered. As a result, if we see that the illuminated portions of the (50 km)^2 areas are systematically brighter than their shadowy portions, 3D effects should be held responsible for the systematic difference.

The presented technique's second limitation is that it detects only one component of the overall 3D effects (the asymmetry) and does not give direct information on their other aspects such as radiative smoothing (e.g., Marshak et al. 1995b). This problem becomes especially important when the sun is nearly overhead. In this case the direction of a cloud slope cannot make much of a difference, and so our technique cannot detect illuminated–shadowy differences even if other 3D effects are present. Recognizing this deficiency, the paper examines only scenes with solar zenith angles greater than 20°.

Third, the technique relies on the imperfect assumption that slopes tilted toward the sun (termed ''illuminated slopes'' in this paper) are always brightened by 3D effects, and that slopes tilted away from the sun (termed ''shadowy slopes'') are always darkened. The resulting random misclassification of some pixels into

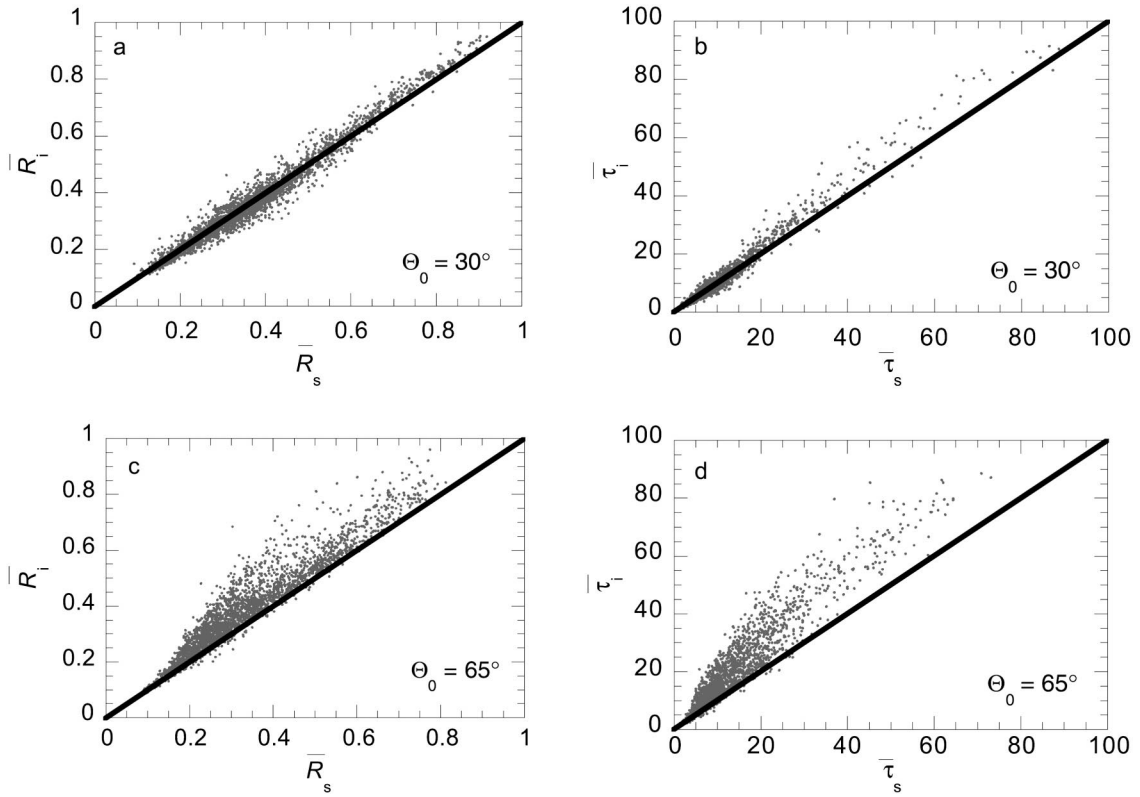

FIG. 3. Comparison of the illuminated and shadowy portions of examined areas. In this graph, each point represents a separate (50 km)^2 area. (a) Reflectance for $\Theta_0 = 30°$, (b) retrieved optical thickness for $\Theta_0 = 30°$, (c) reflectance for $\Theta_0 = 65°$, and (d) retrieved optical thickness for $\Theta_0 = 65°$. In order to reduce statistical uncertainties, only areas with cloud fractions larger than 10% are examined.

the wrong category brings the two category's mean brightnesses closer together, leading to an underestimation of 3D effects. Similarly, if the solar azimuth is not exactly along rows, columns, or diagonal lines in the satellite image, the method must use neighboring pixels that lie not exactly in front or behind our pixel (considering the exact solar direction), and this can also result in some misclassifications, and hence, underestimations of 3D effects. Thus, the results of this simple technique should be regarded as lower-bound estimates of 3D effects.

4. Detection results

Figure 3 displays the direct comparison of mean values obtained for illuminated and shadowy slopes within each of the 2742 examined (50 km)^2 areas. Figure 3a shows that for not-too-bright areas, the two kinds of slopes tend to be similar, indicating the lack of systematic 3D effects. The scatter around the one-to-one line is caused by random factors such as wind shear or the overlap of two different cloud layers. For bright areas, however, illuminated slopes are systematically brighter, which indicates that 3D effects become more important as the cloud brightness increases. This tendency is in agreement with the observations of Loeb and Davies (1996) and the theoretical results of Várnai and Marshak (2001), who also found stronger 3D effects for brighter clouds. Figure 3b shows the consequences for optical thickness retrievals: in thick areas ($\bar{\tau} > 20$), 3D effects cause significant retrieval errors that make illuminated slopes appear thicker than shadowy slopes.

Perhaps the most striking parts are shown in Figs. 3c and 3d. These panels show that 3D effects become much stronger when the sun is more oblique (e.g., Loeb and Davies 1996) and that they dominate over random asymmetries even for thin clouds.

Let us now examine the frequency at which various relative differences between illuminated and shadowy slopes occur. The relative difference (D_r) is defined as the ratio of the difference to the mean value, calculated using the equation

$$D_r = \frac{(\bar{\tau}_i - \bar{\tau}_s)}{\left(\frac{\bar{\tau}_i + \bar{\tau}_s}{2}\right)}. \quad (3)$$

As one might expect from Fig. 3b, the histogram of asymmetries for $\Theta_0 = 30°$ is dominated by random scatter, and so it does not give much information on 3D effects (not shown). For $\Theta_0 = 65°$, however, the asymmetries observed in Fig. 3d appear clearly in the cu-

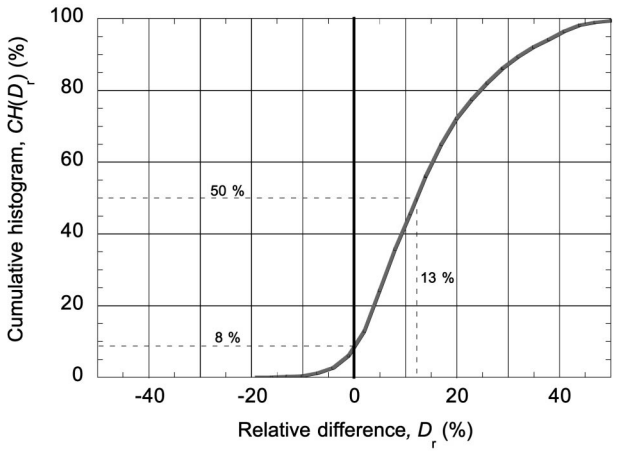

FIG. 4. Cumulative histogram (CH) of the relative difference (D_r) values calculated for each (50 km)^2 area for $\Theta_0 = 65°$. CH(D_r) is defined as the probability that, for any randomly chosen area, the relative difference lies between $-\infty$ and D_r.

mulative histogram (Fig. 4). The figure shows that random asymmetries make shadowy slopes appear brighter than illuminated slopes in about 8% of areas. Since these random effects are unlikely to move the median value significantly, the figure also indicates that in half of the areas, 3D effects make illuminated slopes appear thicker than shadowy slopes by more than 13%. And although the random effects certainly contribute to the largest relative difference values (thereby making the cumulative histogram curve a bit more gradual than 3D effects alone would), the figure clearly shows that 3D effects are important in a substantial portion of clouds.

5. Estimation of 3D effects for individual pixels

This section describes a technique that can estimate 3D effects not only for large, (50 km)^2 areas, but also for (1 km)^2 pixels. While we do not expect the results to be accurate for each individual pixel, the method proposed in this section is affected less by the limitations of the technique discussed in section 3, and it allows a more detailed statistical analysis of 3D effects, such as how they depend on various environmental and cloud parameters. The high-resolution estimates could also be used to adjust the results of 1D retrievals in future studies, with the goal of removing the artificial asymmetry of clouds and improving upon the large-scale mean and standard deviation of the retrieved τ fields. After further refinements and rigorous testing, the pixel-by-pixel estimates of 3D effects can serve as pixel-by-pixel uncertainty estimates for the operational 1-km-resolution cloud optical thickness product (considering only the uncertainties due to 3D effects).

Because this section focuses on (1 km)^2 pixels, all quantities will refer to this resolution, unless otherwise noted. Quantities with overbars indicate averages of (1 km)^2 values over (50 km)^2 areas.

To define the influence of 3D effects, let us consider a (1 km)^2 pixel in a heterogeneous cloud. As a starting point, let us assume that we know the properties of the pixel and its surroundings exactly, including the variability at subpixel scales. Then, ideally, we can use a perfect 3D radiative transfer model to calculate the pixel's observable reflection shaped by 3D radiative effects (R_{3D}). In addition, we can also perform a horizontal averaging of cloud properties over the pixel's area to get its mean optical thickness (τ_{1D}) and then calculate the corresponding 1D reflectance (R_{1D}) using the 1D radiative transfer function (f_{1D}) that connects the optical depth and reflectance values:

$$R_{1D} = f_{1D}(\tau_{1D}). \tag{4}$$

The influence of 3D effects on a pixel's 0.86-μm reflectance (ΔR) is then defined as

$$\Delta R = R_{3D} - R_{1D}. \tag{5}$$

Because satellite retrievals are based on 1D theory, they take the measured values of R_{3D} and retrieve the corresponding τ_{3D} value using the inverse function of f_{1D}:

$$\tau_{3D} = f_{1D}^{-1}(R_{3D}). \tag{6}$$

Note that here the pixel's true (but in practice, unknown) optical thickness is τ_{1D}, whereas τ_{3D} is the retrieved value that may be biased due to 3D effects. Therefore the influence of 3D effects on the retrieved τ values ($\Delta\tau$) can be defined as

$$\Delta\tau = \tau_{3D} - \tau_{1D}. \tag{7}$$

a. Estimating the influence of 3D effects on reflectance ΔR

The influence of 3D effects is calculated by separating the overall effect into two components that are odd and even functions of the temperature gradient g:

$$\Delta R = \Delta R_o + \Delta R_e, \tag{8}$$

such that

$$\Delta R_o(g) = -\Delta R_o(-g), \quad \text{and} \tag{9}$$

$$\Delta R_e(g) = \Delta R_e(-g). \tag{10}$$

This separation is useful because the observations tell us the magnitude of ΔR_o directly, and then we can use empirical relationships between the two components [established in section 5a(2)] to get ΔR_e. The reason that observations can reveal ΔR_o is that only this component affects illuminated and shadowy slopes differently [according to Eq. (10), ΔR_e affects them the same way], and so the measured brightness differences between the two kinds of slopes can be attributed entirely to ΔR_o.

For the sake of simplicity, the proposed method will be described using the local temperature gradient g as

a measure of local cloud sloping. For the approximately 20% of cloudy pixels that lie at cloud edges, however, the temperature gradient would be dominated by the temperature jump between cloudy and clear pixels, which has much more to do with cloud-base altitude than with 3D effects occurring in clouds. Therefore, the gradient in retrieved cloud optical thickness is used instead for these pixels.

1) THE ODD COMPONENT, ΔR_o

The basic idea of the proposed technique is to use a certain area around the pixel [e.g., $(51\ \text{km})^2$] to establish a statistical relationship between g [defined by Eq. (2)] and the 0.86-μm reflectance, and to apply this relationship to estimate ΔR_o for the pixel we are considering. Because the relationship may change with cloud thickness, the statistical relationship is established using only those pixels whose brightness temperature is sufficiently close to our pixel's.

In order to illustrate that the local gradient values are indeed related to the 3D effects, Fig. 5a shows a sample cloud field, and Fig. 6 shows R_{3D} as a function of g for this scene. Figure 6 suggests that there is a statistical relationship between the two quantities. The scatter of points around a single $R_{3D}(g)$ curve can be attributed to variations in factors other than 3D effects (such as the cloud volume extinction coefficient) and to the fact that the local temperature gradient (g) does not determine the magnitude of 3D effects completely. (For example, variability in directions perpendicular to the sun can also change 3D effects, to a lesser degree.)

The assumed linear relationship between g and R_{3D} can be written in the form

$$R_{3D}(g) = C_1 g + C_2, \tag{11}$$

where C_1 and C_2 are regression coefficients defined below. A linear R–g relationship is assumed because simple trigonometric calculations revealed that in symmetrical clouds, the difference in the solar radiation intercepted by slopes tilted toward and away from the sun depends on the steepness of the slopes (i.e., on g) nearly linearly.

If the relationship is established through a linear interpolation that is based on the average values of illuminated and shadowy pixels, then

$$R_{3D}(g) = \overline{R}_s + \frac{\overline{R}_i - \overline{R}_s}{\overline{g}_i - \overline{g}_s}(g - \overline{g}_s), \tag{12}$$

where $\overline{g}_i$ and $\overline{g}_s$ are the mean gradient values for illuminated and shadowy pixels, respectively. The comparison of Eqs. (11) and (12) then reveals that

$$C_1 = \frac{\overline{R}_i - \overline{R}_s}{\overline{g}_i - \overline{g}_s}, \quad \text{and} \tag{13}$$

$$C_2 = R_{3D}(0). \tag{14}$$

We can now define ΔR_o as the estimated influence of the cloud slope on R_{3D}:

$$\Delta R_o(g) = R_{3D}(g) - R_{3D}(0) = C_1 g = \frac{\overline{R}_i - \overline{R}_s}{\overline{g}_i - \overline{g}_s} g. \tag{15}$$

2) THE EVEN COMPONENT ΔR_e

A simple rearrangement of Eq. (8) can provide us a definition of ΔR_e as the difference between a pixel's reflectances in 3D and 1D theory minus the ΔR_o component calculated above.

Although the direct comparison of illuminated and shadowy slopes cannot reveal brightness changes that affect both kinds of pixels the same way, observations of the asymmetry can still be used to estimate this component. The idea is to relate the aspect of 3D effects that we observe (the asymmetry) to their other aspects (e.g., the shift in average brightness) through theoretical simulations.

In order to see whether or not a such relationship exists, we performed Monte Carlo simulations over a wide variety of fractal cloud fields described by Várnai and Marshak (2001). Figure 7 shows that the observed $\overline{R}_i - \overline{R}_s$ difference is closely related to the shift in average brightness. As expected from earlier studies, the mean brightness is increased by 3D effects for very oblique sun (e.g., Loeb et al. 1997; Várnai and Davies 1999), and it is reduced for small solar zenith angles (e.g., Davis and Marshak 2001). The area average shift ($\overline{\Delta R_e}$) can thus be related to the observed asymmetry through

$$\overline{\Delta R_e} = b(\Theta_0)(\overline{R}_i - \overline{R}_s), \tag{16}$$

where $b(\Theta_0)$ is an empirical function. The inset in Fig. 7 shows that $b(\Theta_0)$ can be approximated as

$$b(\Theta_0) = m_1 - m_2 \cos\Theta_0, \tag{17}$$

where $m_1 = 0.57 \pm 0.1$ and $m_2 = 1.32 \pm 0.16$.

Once we obtained the area average value of ΔR_e from Eq. (16), we can distribute it among the individual pixels the following way. First, we need to consider the physical requirement that ΔR_e should be zero in the homogeneous areas and that it should be increasingly strong in more and more heterogeneous regions. The degree of heterogeneity—that is, the susceptibility of each pixel to 3D effects—can be best described by ΔR_o for that pixel. In addition, since ΔR_e is an even function of g, it can depend only on the absolute value, but not the sign, of ΔR_o. Thus, for individual pixels we can write

$$\Delta R_e(g) = \frac{\overline{\Delta R_e}|\Delta R_o|}{|\overline{\Delta R_o}|} = \frac{b(\Theta_0)(\overline{R}_i - \overline{R}_s)|g|}{|\overline{g}|}. \tag{18}$$

Finally, the overall estimate of 3D effects on reflectance, ΔR, can be calculated by combining Eqs. (8), (15), and (18):

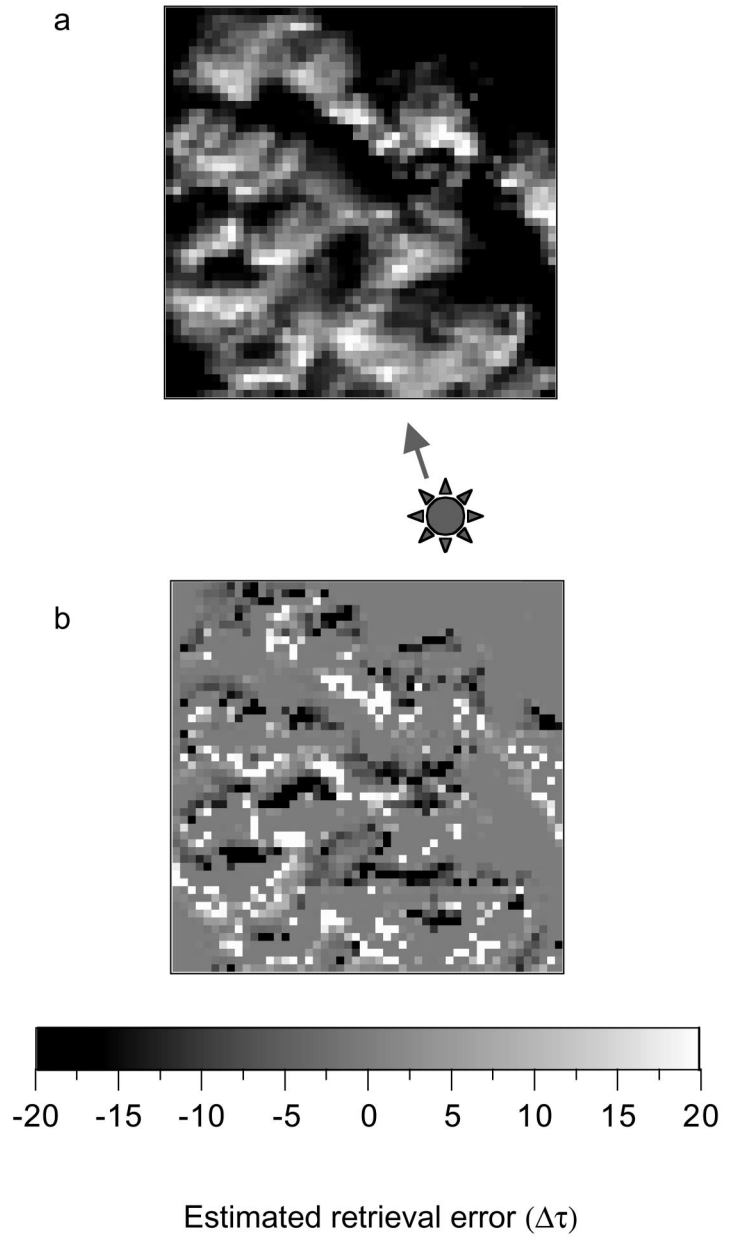

FIG. 5. (a) A sample (51 km)^2 cloud field over the North Atlantic ocean (in the granule observed at 1305 UTC 1 Nov 2000) for $\Theta_0 = 75°$. The cloud fraction is 78%, and the average cloud optical thickness is 39. (b) The estimated influence of 3D effects on 1-km-resolution τ retrievals. (See section 6.)

$$\Delta R = \Delta R_o + \Delta R_e = \frac{\overline{R}_i - \overline{R}_s}{\overline{g}_i - \overline{g}_s} g + \frac{b(\Theta_0)(\overline{R}_i - \overline{R}_s)|g|}{|\overline{g}|}. \quad (19)$$

In the end, let us restate the two main physical assumptions used for the estimations of ΔR.

- A pixel's reflectance depends linearly on the local temperature gradient g [see Fig. 6 and Eq. (12)].
- The shift in the area average reflectance is proportional to the observed asymmetry of cloud reflectance [see Fig. 7 and Eq. (18)].

b. *Influence of 3D effects on retrieved τ values $\Delta\tau$*

Once the influence of 3D effects on the measured reflectances is obtained, the proposed algorithm's next task is to estimate the influence on the retrieved optical

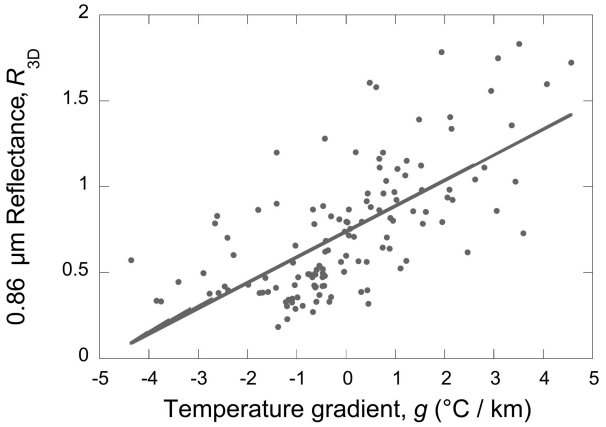

FIG. 6. The relationship between reflectance and local temperature gradient for all pixels in the field in Fig. 5 that have brightness temperatures between 278 and 279 K. The solid line indicates a linear fit to the data.

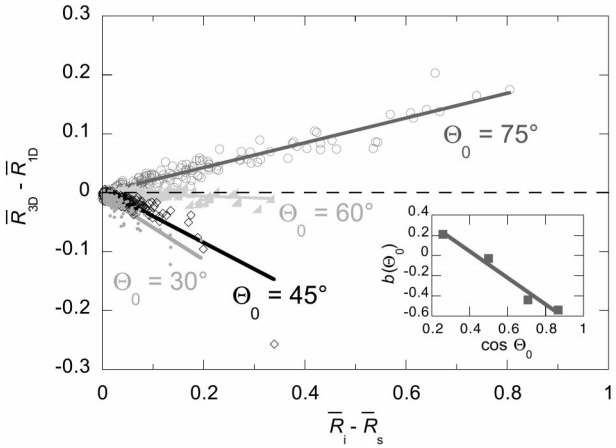

FIG. 7. The relationship between the separation of illuminated and shadowy pixels and the shift in scene-average brightness in 3D Monte Carlo simulations. Each data point represents simulation results for a separate (50 km)^2 scene. Results for four different solar zenith angles are displayed. The inset shows how the slope of the linear fits (b) depends on the solar zenith angle (Θ_0) (see text for discussion).

thickness values $\Delta\tau$. In principle, one could use the operational MODIS algorithm to estimate how the retrieved optical thickness values would change if the measured brightnesses were adjusted to counter the influence of 3D effects (i.e., shifted by $-\Delta R$). However, because incorporating the operational MODIS code into our program would have been a daunting task, we used the following efficient yet simple procedure instead.

The procedure relies on the fact that in 1D theory, the visible brightness has a nearly one-to-one relationship with the optical thickness. Therefore, our procedure starts by taking the cloudy pixels within the (51 km)^2 area surrounding our pixel and then building a local lookup table (lut) that contains the mean value of optical thicknesses retrieved for pixels that fall into various narrow brightness bins. (For self-consistency, only those surrounding pixels are considered that have the same cloud phase and underlying surface type as the pixel being examined—in this case, ocean.) Then the procedure generates an initial estimate of τ_{1D} (marked τ_{1D}^{lut}) by first calculating

$$R_{1D} = R_{3D} - \Delta R, \tag{20}$$

then finding in the lookup table the two brightness values closest to our pixel's calculated R_{1D} value (marked as *lower* and *higher*), and finally, using a simple linear interpolation:

$$\tau_{1D}^{lut} = \tau_{lower}^{lut} + (\tau_{higher}^{lut} - \tau_{lower}^{lut})\frac{R_{1D} - R_{lower}^{lut}}{R_{higher}^{lut} - R_{lower}^{lut}}. \tag{21}$$

In the case of exceptions for which interpolation cannot be used, an extrapolation is performed in a similar manner. The final estimate of τ_{1D} is then obtained by determining what τ_{3D}^{lut} value would correspond to the actual measurement R_{3D} in our lookup table, and then using the equation

$$\tau_{1D} = \tau_{1D}^{lut} + (\tau_{3D} - \tau_{3D}^{lut}). \tag{22}$$

Although the difference ($\tau_{3D} - \tau_{3D}^{lut}$) is usually small, it improves upon our initial guess, τ_{1D}^{lut}. This correction term considers that the current pixel may have slightly different parameter values (e.g., droplet size) than the mean parameters are over the (51 km)^2 area that we used for constructing the lookup table.

c. *Influence of subpixel variability*

As indicated by earlier studies (e.g., Davis et al. 1997; Oreopoulos and Davies 1998), subpixel variability can cause systematic retrieval biases [called plane-parallel bias after Cahalan et al. (1994)] even when no 3D effects are present: the nonlinear relationship between τ and R can result in the underestimation of the average τ value.

Fortunately, the estimates of 3D effects consider this plane-parallel bias as well, because the Monte Carlo simulations in Fig. 7 include the effects of subpixel variability. However, we still need an alternative technique to estimate the plane-parallel bias for the cases in which the 3D detection algorithm cannot work (e.g., small solar zenith angles).

Specifically, we use the 3D estimation technique described above whenever the solar zenith angle is greater than 45°. If the solar zenith angle is between 20° and 45°, we start by averaging the τ values in the (51 km)^2 area that surrounds our pixel. If this average is greater than 20, we still use the 3D estimation method. If, however, the average value is less than 20, we declare that the observed asymmetry between illuminated and shadowy slopes does not show the true 3D effects (see Fig. 3b). Therefore, we use the technique outlined below instead and report the plane-parallel bias as our most reliable estimate of horizontal cloud heterogeneity effects. Similarly, the plane-parallel bias is reported whenever the solar zenith angle is less than 20°.

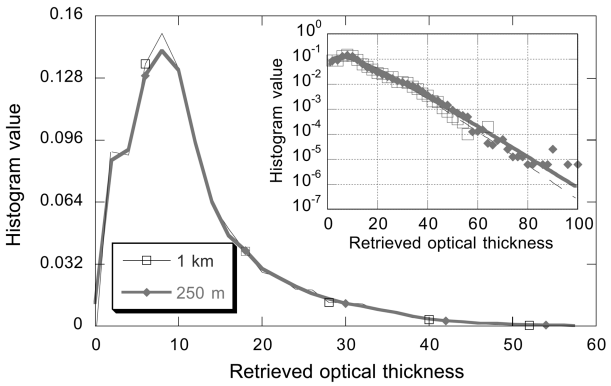

FIG. 8. Comparison of the histograms of optical thickness values retrieved at 250-m and 1-km resolution over a sample area that contains a broken cumulus field. The cloud fraction is 90%, and the solar zenith angle is 33°. The inset shows the histograms on a logarithmic scale, which is more suitable for examining the histograms' wings at large τ values. The filled diamonds and empty squares show results for 250-m and 1-km resolutions, respectively. The values for 1-km resolution drop to 0 around $\tau = 65$, whereas the tail of the 250-m distribution reaches much further. In the inset, the solid and dashed lines display gamma distributions fit to the 250-m- and 1-km-resolution data.

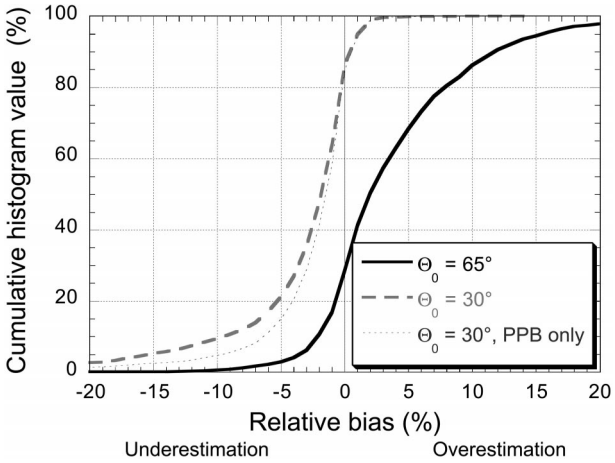

FIG. 9. Cumulative histogram of estimated retrieval errors for the mean optical thickness of (50 km)^2 areas. For $\Theta_0 = 30°$, the dashed curve displays the overall results of the proposed technique, and the dotted curve shows the results if only the plane-parallel bias is calculated (even for areas with $\overline{\tau} > 20$), without considering any 3D effects.

We get simple first-order estimates of the plane-parallel bias by examining the 250-m reflectances that MODIS provides at the 0.86-μm wavelength. The influence can be obtained by building local lookup tables of corresponding R and τ values much the same way as in section 5b, and using this table to estimate how the retrieved optical thickness values would change ($\Delta\tau_{\text{ppb}}$) if we used input data at 250-m (and not 1 km) resolution:

$$\Delta\tau_{\text{ppb}} = \overline{\overline{\tau_{250\text{ m}}}} - \tau_{1\text{ km}}, \tag{23}$$

where the double overbar indicates averaging over the area covered by the (1 km)^2 pixel. Let us note that this simple method can be trusted only for small solar zenith angles: for oblique sun, 3D effects make clouds appear overly structured, which can lead to an overestimation of $\Delta\tau_{\text{ppb}}$ (Zuidema and Evans 1998; Várnai 2000).

In order to illustrate the influence of spatial resolution, Fig. 8 compares the histograms of τ values retrieved at 1-km and 250-m resolutions for a sample scene. The figure shows that 1-km-resolution retrievals yield a narrower range of τ values; their histogram has smaller values at the edges (at $\tau < 2$ and $\tau > 40$) and higher values near the peak of the histogram ($5 < \tau < 10$). Although the histograms for the two resolutions have similar shapes and mean values (11.7 versus 11.8), their standard deviations are significantly different: 8.3 at 1 km versus 8.8 at 250 m. Part of the difference arises simply because averaging the true τ values from 250-m to 1-km resolution should indeed reduce the variability—that is, variability truly depends on the scale at which it is considered.

In addition, the plane-parallel bias also contributes to 1-km retrievals giving smaller variability values. This bias can be removed by using Eq. (23), that is, by first retrieving τ values at 250-m resolution and then averaging the results over (1 km)^2 pixels. For the sample scene, this procedure gives an intermediate standard deviation of 8.5.

Finally, the inset in Fig. 8 shows that gamma distributions (e.g., Barker 1996) describe well the long tail of the optical thickness distributions toward high τ values.

6. Estimation results

Figure 5b shows an example of results from the technique described in section 5. The figure illustrates the tendency for 1D retrievals to overestimate optical thickness on the cloud sides facing the sun and to underestimate it on the opposite sides. As Zuidema and Evans (1998) and Várnai (2000) noted, this means that cloud fields appear artificially asymmetric and overly structured in the retrieved images.

While the examination of individual scenes can give important insights into the workings of 3D effects, at this point it is perhaps more interesting to examine how cloud heterogeneities change the statistical properties of the retrieved cloud fields. Although we cannot obtain accurate global statistics from the limited number of MODIS images we have, we can still use these scenes to address general question such as the following.

- Are 3D effects important in practice, or can they be neglected in most cases?
- Do the errors caused by 3D effects cancel out when we average the results over large areas?

Figure 9 shows that in many cases, retrieval errors

remain significant even if the pixel-by-pixel results are averaged over (50 km)^2 areas. Since $\overline{\tau} < 20$ for most (50 km)^2 areas (Fig. 3b), the results for $\Theta_0 = 30°$ are shaped mainly by estimations of subpixel variability effects, that is, by the plane-parallel bias. The errors for $\Theta_0 = 30°$ are mostly underestimations for two reasons. First, the convex shape of the 1D radiative transfer function $R(\tau)$ implies that the plane-parallel bias causes underestimations (e.g., Davis et al. 1997). The second reason is that for high sun, 3D effects tend to reduce the area-average brightness values (see Fig. 7), which further strengthens the underestimations.

However, for $\Theta_0 = 30°$, Fig. 9 shows a conservative lower bound estimate of the influence of cloud heterogeneity. Our estimates consider subpixel variability only at scales larger than 250 m, and the current algorithm cannot estimate 3D effects for $\overline{\tau} < 20$. Because the cumulative histogram value around 10% underestimation is changed significantly by 3D effects even though it is calculated only for areas with $\overline{\tau} > 20$, we expect that the estimated biases would increase if we were able to calculate 3D effects for all areas.

Figure 9 also shows that the tendency reverses for oblique sun, and overestimations become predominant. One reason for the reversal is that for $\Theta_0 > 65°$, 3D effects increase, not decrease, the area average reflectance (see Fig. 7). An additional reason for the overestimations is that 3D effects make clouds appear more heterogeneous than they really are, which causes an effect similar to the plane-parallel bias, but with the opposite sign. (The plane-parallel bias's underestimations occur when clouds appear too homogeneous on satellite images that cannot resolve small-scale cloud variability.) Finally, random effects also contribute to both the underestimations and the overestimations. For example, wind shear or the random arrangement of clouds can make individual (50 km)^2 areas contain more illuminated or shadowy pixels, which means that overestimations or underestimations will become more abundant in that particular area.

In addition to changing the area average values, heterogeneity effects can also change higher-order moments (e.g., standard deviation and skewness) of the retrieved cloud fields (e.g., Várnai 2000). The effects on standard deviation become especially important if this parameter is used to characterize large-scale cloud variability in climate studies (e.g., Barker 1996; Oreopoulos and Barker 1999; Pincus et al. 1999). Figure 10 shows that for high sun, the retrievals tend to underestimate the standard deviation of 1-km-resolution τ values in (50 km)^2 areas. Most of the underestimations is a direct consequence of the reduction in mean τ values shown in Fig. 9. If the τ values are too low in general, their spread can also be expected to become smaller. The figure also shows that for oblique sun, overestimations of cloud variability become dominant. One reason is that τ values are overestimated in general (see Fig. 9), and another is that the more abundant 3D effects

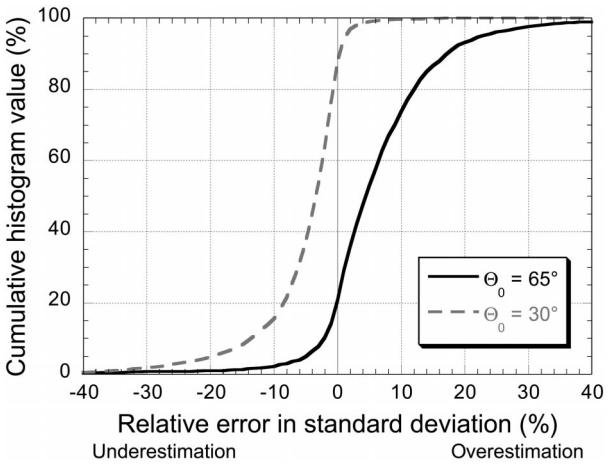

FIG. 10. Cumulative histogram of estimated errors in the standard deviation of 1-km-resolution τ values over (50 km)^2 areas. As in all other figures, cloud-free pixels were not included in the calculations of statistical parameters.

make clouds appear overly heterogeneous. Because 3D effects act in opposite directions for high sun and oblique sun (in both Figs. 10 and 11), one can expect unbiased results for intermediate solar zenith angles ($\Theta_0 \approx 40°$–$50°$).

The degree of cloud heterogeneity can also be characterized through the parameter η,

$$\eta = 1 - \chi = 1 - \frac{\exp(\overline{\ln\tau})}{\overline{\tau}}, \qquad (24)$$

which varies between 0 for homogeneous clouds and 1 for extreme variability (e.g., δ functions). The parameter χ was introduced by Cahalan et al. (1994). The η calculations for all (50 km)^2 areas in the $\Theta_0 = 30°$ scenes yielded overall average values of 0.15 and 0.13 for the 250-m- and 1-km-resolution τ fields, respectively. This means that, measured by this parameter, 250-m-resolution clouds are 10% more heterogeneous than their 1-km-resolution counterparts.

Finally, it may be interesting to compare the proposed technique's error estimates to the estimates of an earlier method described in Várnai and Marshak (2001). That method used theoretical simulations over a wide range of artificially generated cloud fields to set error bounds on the retrieved τ values. Ideally, the one σ level error bounds should mark the confidence interval that contains the pixel's true optical thickness with a 68% probability, which implies that (100%–68%)/2 = 16% of pixels may have actual values outside the error bounds on both the underestimation and overestimation sides. Figure 11 compares the earlier method's error bounds with the current technique's error estimates for all pixels with retrieved τ values between 18 and 22. The figure shows that because the error bounds [calculated from Eq. (2) of Várnai and Marshak (2001)] depend only on the solar elevation and the retrieved τ value of the pixel, they vary in a narrow range around five. The agreement

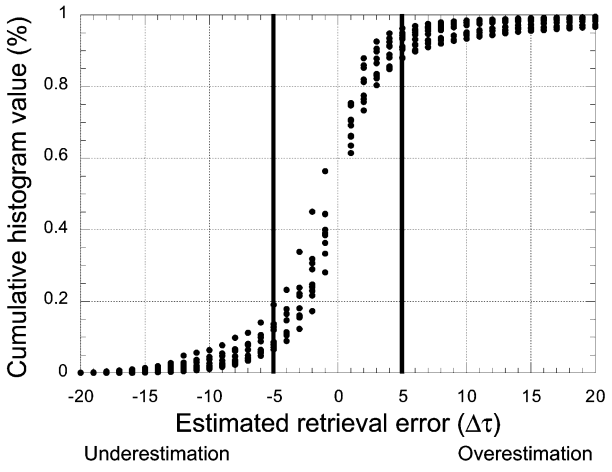

FIG. 11. A comparison of the error bounds of Várnai and Marshak (2001) to the τ retrieval errors estimated by the technique proposed in this paper. The vertical solid lines indicate the average error bounds, and the dots indicate the cumulative histogram of estimated τ retrieval errors for each of the 10 MODIS images for $\Theta_0 = 65°$.

between the old and new techniques is remarkably good. Still, the current method is much more advanced: it takes advantage of more information about a particular scene, and it estimates not only the magnitude, but also the sign of 3D effects.

7. Summary

This paper addressed two questions on how 3D cloud heterogeneities influence satellite retrievals of cloud properties. First, it proposed an algorithm that allows us to estimate the influence of 3D radiative effects on 1-km-resolution retrievals of cloud optical thickness (τ), and second, it examined 20 MODIS images to see whether the influence is important in real clouds or can be neglected in most situations.

The proposed technique used a twofold approach. When possible, it combined visible (0.86 μm) and thermal infrared (11 μm) images to see whether 3D radiative effects make clouds appear asymmetric, that is, whether cloud slopes tilted toward the sun are systematically brighter than those tilted away from it. Systematic asymmetries would indicate that considering one pixel at a time in 1D retrievals cannot give accurate results. One also needs to consider the local gradients that influence 3D radiative interactions among neighboring pixels. When this approach cannot be used because the sun is too close to the zenith (and so the direction of cloud slopes cannot make much difference), the technique estimates the influence of cloud heterogeneities from the variability of (250 m)^2 pixels inside each (1 km)^2 pixel. Considering this small-scale variability results in retrievals that estimate clouds to be thicker and more variable, with wider probability distribution functions of τ values.

The proposed technique took a conservative approach to estimating heterogeneity effects, thus yielding cautious, lower bound estimates. The fact that one of the described methods uses theoretical simulations to some degree can raise the question of whether the simulations were sufficiently realistic or not. Fortunately, the results of even this method were not affected by whether the simulated cloud fields were too heterogeneous or homogeneous, because the simulated fields were used only to establish a statistical relationship between two components of 3D effects that vary together with the magnitude of cloud heterogeneity: the clouds' observed asymmetry and the estimated shift in area average brightness.

Because the proposed technique estimates 3D effects for each individual (1 km)^2 pixel, it can be used to estimate the uncertainties of operational τ retrievals. Although the estimates are not expected to be perfectly accurate for each individual pixel, performing the calculations at a high spatial resolution makes the method more accurate in estimating statistical properties of large areas. Eventually, the technique could even be used to compensate for heterogeneity effects in the retrievals by adjusting the pixels' retrieved τ values according to the estimated heterogeneity effects. This correction would remove the artificial asymmetry of clouds and improve upon the large-scale mean and standard deviation of the retrieved τ fields.

After describing the proposed technique, the paper examined 20 randomly selected MODIS scenes over oceanic areas (each scene covering an area of 2000 km by 450 km). Although this limited dataset cannot be expected to yield reliable global statistics on radiative heterogeneity effects, it gives initial impressions about whether cloud heterogeneity effects are important in practice.

The results indicated that 3D radiative effects occur quite frequently. For example, when the scenes were divided into (50 km)^2 areas, a majority of the areas were affected for solar zenith angles around 65°. (In more than half of the areas, 3D effects made slopes tilted toward the sun appear at least 10% brighter than similar slopes tilted away from the sun.)

Finally, the results pointed out that heterogeneity effects influencing (1 km)^2 pixels do not cancel out when τ values are averaged over (50 km)^2 areas. The area mean τ values were biased by more than 10% in about 10% of the areas, and the errors in the areas' standard deviation values were more than 10% in about 20% of the areas. However, since these results were obtained through a conservative algorithm, we expect that the real magnitude of heterogeneity effects is larger than these estimates. Also, since the biases were in opposite directions for high and low sun, one can expect unbiased results for intermediate solar elevations.

Future studies could extend the present conservative estimates by also providing more balanced estimates in which underestimations and overestimations of 3D effects are equally likely. For this, the current technique

should be extended to estimate the entire heterogeneity effects for all solar zenith angles. Additional improvements could be made by adjusting the technique's parameters for optimal sensitivity, for example by changing the size of the surrounding areas that are used to estimate 3D effects for $(1\ \text{km})^2$ pixels. Finally, future studies could also explore extending the proposed method to oblique view directions.

Acknowledgments. We appreciate funding for this research from the NASA EOS Project Science Office (under Grant NAG5-6675) and support from project scientist David O'C. Starr. We also thank Laura L. Atwood for proofreading the manuscript and providing helpful suggestions.

REFERENCES

Barker, H. W., 1996: A parameterization for computing grid-averaged solar fluxes for inhomogeneous marine boundary layer clouds. Part I: Methodology and homogeneous biases. *J. Atmos. Sci.*, **53,** 2289–2303.

——, and D. Liu, 1995: Inferring optical depth of broken clouds from Landsat data. *J. Climate*, **8,** 2620–2630.

Cahalan, R. F., W. Ridgway, W. J. Wiscombe, T. L. Bell, and J. B. Snider, 1994: The albedo of fractal stratocumulus clouds. *J. Atmos. Sci.*, **51,** 2434–2455.

Davies, R., 1984: Reflected solar radiances from broken cloud scenes and the interpretation of satellite measurements. *J. Geophys. Res.*, **89,** 1259–1266.

Davis, A., and A. Marshak, 2001: Multiple scattering in clouds: Insights from three-dimensional diffusion/P1 theory. *Nucl. Sci. Eng.*, **137,** 251–280.

——, ——, R. Cahalan, and W. Wiscombe, 1997: The Landsat scale break in stratocumulus as a three-dimensional radiative transfer effect: Implications for cloud remote sensing. *J. Atmos. Sci.*, **54,** 241–260.

King, M. D., S.-C. Tsay, S. Platnick, M. Wang, and K.-N. Liou, 1997: Cloud retrieval algorithms for MODIS: Optical thickness, effective particle radius, and thermodynamic phase. MODIS Algorithm Theoretical Basis Doc. ATBD-MOD-05, 79 pp.

Kobayashi, T., 1993: Effects due to cloud geometry on biases in the albedo derived from radiance measurements. *J. Climate*, **6,** 120–128.

Loeb, N. G., and R. Davies, 1996: Observational evidence of plane parallel model biases: Apparent dependence of cloud optical depth on solar zenith angle. *J. Geophys. Res.*, **101,** 1621–1634.

——, and J. A. Coakley, 1998: Inference of marine stratus cloud optical depths from satellite measurements: Does 1D theory apply? *J. Climate*, **11,** 215–233.

——, T. Várnai, and R. Davies, 1997: Effect of cloud inhomogeneities on the solar zenith angle dependence of nadir reflectance. *J. Geophys. Res.*, **102,** 9387–9395.

Marshak, A., A. Davis, W. Wiscombe, and R. Cahalan, 1995a: Radiative smoothing in fractal clouds. *J. Geophys. Res.*, **100,** 26 247–26 261.

——, ——, ——, and G. Titov, 1995b: The verisimilitude of the independent pixel approximation used in cloud remote sensing. *Remote Sens. Environ.*, **52,** 72–78.

Nakajima, T. Y., and M. D. King, 1990: Determination of the optical thickness and effective radius of clouds from reflected solar radiation measurements. Part I: Theory. *J. Atmos. Sci.*, **47,** 1878–1893.

NASA, cited 2000: MODIS—Moderate-Resolution Imaging Spectroradiometer. [Available online at http://eospso.gsfc.nasa.gov/eos_homepage/Instruments/MODIS/.]

Oreopoulos, L., and R. Davies, 1998: Plane parallel albedo biases from satellite observations. Part II: Parameterizations for bias removal. *J. Climate*, **11,** 933–944.

——, and H. W. Barker, 1999: Accounting for subgrid-scale cloud variability in a multi-layer 1D solar radiative transfer algorithm. *Quart. J. Roy. Meteor. Soc.*, **125,** 301–330.

——, A. Marshak, R. F. Cahalan, and G. Wen, 2000: Cloud 3D effects evidenced in Landsat spatial power spectra and autocorrelation functions. *J. Geophys. Res.*, **105,** 14 777–14 788.

Pincus, R., S. A. McFarlane, and S. Klein, 1999: Albedo bias and the horizontal variability of clouds in subtropical marine boundary layers: Observations from ships and satellites. *J. Geophys. Res.*, **104,** 6183–6191.

Thomas, G. E., and K. Stamnes, 1999: *Radiative Transfer in the Atmosphere and in the Ocean.* Cambridge University Press, 517 pp.

Várnai, T., 2000: Influence of three-dimensional radiative effects on the spatial distribution of shortwave cloud reflection. *J. Atmos. Sci.*, **57,** 216–229.

——, and R. Davies, 1999: Effects of cloud heterogeneities on shortwave radiation: Comparison of cloud-top variability and internal heterogeneity. *J. Atmos. Sci.*, **56,** 4206–4223.

——, and A. Marshak, 2001: Statistical analysis of the uncertainties in cloud optical depth retrievals caused by three-dimensional radiative effects. *J. Atmos. Sci.*, **58,** 1540–1548.

Zuidema, P., and K. F. Evans, 1998. On the validity of the independent pixel approximation for the boundary layer clouds observed during ASTEX. *J. Geophys. Res.*, **103,** 6059–6074.